



Single-Photon-Induced Post-Ionization to Boost Ion Yields in MALDI Mass Spectrometry Imaging**

Christoph Bookmeyer, Ulrich Röhling[†], Klaus Dreisewerd, and Jens Soltwisch*

Abstract: Matrix-assisted laser desorption/ionization mass spectrometry imaging (MALDI-MSI) is a rapidly growing method in the life sciences. However, for many analyte classes, its sensitivity is limited due to poor ionization efficiencies. To mitigate this problem, we here introduce a novel post-ionization scheme based on single-photon induced chemical ionization using pulsed RF-Kr lamps. The fine-vacuum conditions of a dual ion-funnel ion source effectively thermalize the evolving MALDI plume and enable ample gas-phase reactions. Injected chemical dopants crucially support fragmentless ionization to $[M+H]^+/[M-H]^-$ species. Based on this interplay, numerous glycerophospho-, sphingo-, and further lipids, registered from mammalian tissue sections, were boosted by up to three orders of magnitude, similar to results obtained with laser-based post-ionization (MALDI-2). Experiments with deuterated matrix and dopant, however, indicated complex chemical ionization pathways different from MALDI-2.

“soft” desorption/ionization technique in MSI applications is matrix-assisted laser desorption ionization (MALDI).^[5] Most commercially available MALDI-MSI instruments now provide a lateral resolution in the range of 5–20 μm , and recent methodological developments demonstrated the potential of MALDI-MSI with a pixel size of about 1 μm and smaller.^[6,7] A notable limitation of the method are low MALDI ion yields—especially in high-resolution applications, where only minute amounts of material are available per pixel. It is estimated that for numerous analyte classes less than one in a million of the ejected molecules are concomitantly ionized.^[8] In addition, molecules with high ion affinities can cause ion suppression effects by abstracting charges from other compounds during the MALDI process. Common examples for ion suppression are phosphatidylcholines (PC), which in the positive ion mode notoriously hamper the detection of the many other lipid classes present in complex tissues.^[9,10]

To meet these challenges, various post-ionization (PI) techniques have been developed, fostering the analytical depths of an experiment.^[11,12] In this regard, several methods based on charge distribution reactions have recently been introduced that enable increased ionization efficiencies for a much broader range of analytes.^[13,14] Because these methods are based on gas-phase reactions between neutrally desorbed analyte molecules and separately ionized charge donors, they require elevated pressure conditions, typically in the range of a few mbar or even atmospheric pressure. Most prominently, a method coined MALDI-2 utilizes an additional pulsed ultraviolet (UV) laser to irradiate the expanding MALDI plume to effectively post-ionize neutral matrix molecules in a two-photon ionization process under fine vacuum conditions.^[14–16] The resulting confinement of the expanding MALDI plume leads to the formation of a temporary reaction vessel and a cascade of secondary MALDI-like ionization reactions. For this scenario, boosts of the ion signal intensities by up to 2–3 orders of magnitude have been reported for numerous analyte classes including lipids, glycans, a range of further metabolites, and pharmaceuticals.^[14–22] In an alternative approach, molecules that are neutrally desorbed during a MALDI-MSI experiment at atmospheric pressure are collected by a stream of gas and allowed to react with ions separately produced in a cold plasma.^[13] Similar to MALDI-2, signal intensities for a number of lipid classes, which notoriously suffer from ion suppression effects, are increased sizably.

Next to utilizing charge transfer reactions, another means for ionizing gaseous molecules is by use of high-energetic vacuum ultraviolet (VUV) light. Here, photon

Introduction

Mass spectrometry imaging (MSI) is a label-free technique that is increasingly used to visualize the spatial distribution of numerous classes of biomolecules, such as lipids, glycans, further metabolites, and pharmaceuticals in biological samples like thin tissue sections.^[1–4] The most widely used

[*] Dr. C. Bookmeyer, Prof. Dr. K. Dreisewerd, Dr. J. Soltwisch
 Institute of Hygiene, University of Münster
 Robert-Koch-Str. 41, 48149 Münster (Germany)
 E-mail: jenssol@uni-muenster.de

U. Röhling
 Institute of Medical Physics and Biophysics, University of Münster
 Robert-Koch-Str. 31, 48149 Münster (Germany)

Dr. C. Bookmeyer
 Metabolomics Interdisciplinary Laboratory, University of Tarragona
 Avinguda Països Catalans 26, 43007 Tarragona (Spain)

[†] Deceased (2021)

[**] A previous version of this manuscript has been deposited on a preprint server (<https://doi.org/10.21203/rs.3.rs-923767/v1>).

© 2022 The Authors. Angewandte Chemie International Edition published by Wiley-VCH GmbH. This is an open access article under the terms of the Creative Commons Attribution Non-Commercial NoDerivs License, which permits use and distribution in any medium, provided the original work is properly cited, the use is non-commercial and no modifications or adaptations are made.

energies of ≈ 10 eV enable efficient single-photon ionization (SPI) of a broad range of biomolecules. Due to an optimal trade-off between low fragmentation rates and high ionization yields, the method has been envisioned as “universal and soft”.^[23] In practice, however, direct SPI often induces at least a certain degree of fragmentation even for small molecule classes,^[24] and the method is typically limited to the analysis of low-weight compounds. Direct SPI is commonly performed in high vacuum ion sources, i.e., to avoid gas-phase reactions of the generated molecular ions. Arguably, the most widely used application of SPI is, however, in atmospheric pressure photoionization (APPI) sources. These utilize such gas-phase reactions in the high particle density to ionize volatile organic compounds (VOC).^[25] Most commonly, dopant vapor (e.g., of acetone or toluene) is added to foster the desired charge transfer reactions between the numerous compounds in close proximity. APPI is powerful for less polar compounds and thus in particular serves to complement electrospray ionization (ESI)-MS measurements.^[25] Another SPI variant, where the ionization takes place in a fine vacuum environment of a few mbar of N_2 , is referred to as low-pressure photoionization (LPPI).^[26] The main advantages of LPPI compared with APPI are reduced side reactions with atmospheric oxygen or nitric compounds and lower degrees of fragmentation due to adiabatic cooling scenarios.^[26] Advantageously, at a few mbar of N_2 , dopant vapor can still straightforwardly be added. Recently, we reported an optimized design of LPPI-MS using Kr discharge lamps in a dual ion funnel-dual MALDI/ESI source. Using a simple capillary-based sample and dopant introduction system, we registered several hundred VOC from exhaled human breath and thousands of (s)VOC from coffee roasts.^[27]

In both APPI and LPPI, the initial photoionization is typically achieved by the use of Kr discharge lamps with main emission lines at 117 and 124 nm (corresponding to photon energies of 10.6 and 10.0 eV). In comparison to lasers of comparable wavelength,^[23] the photon density is considerably lower, and the emission is typically continuous, incoherent, and challenging to focus. As these lamps are much easier to maintain and are more cost-effective than lasers, however, they comprise the most typical light sources for APPI.^[25]

SPI has previously been combined with MALDI in a high-vacuum source to post-ionize amino acid standards.^[28] Here, we report the first application of a pulsed VUV lamp module for efficient PI of a broad range of lipid analytes in a fine-vacuum MALDI-MS imaging setting. A set of fundamental studies performed with deuterated matrix and dopants to analyze lipid standards revealed a high degree of chemical interaction within the confined plume. To account for the fundamental mechanistic differences to those reported for MALDI-2 we will refer to the method in the following as Single-Photon-Induced Chemical Ionization (SPICI). We illustrate the analytical capabilities of MALDI-SPICI-MSI at the examples of mouse brain and kidney sections and of pig brain homogenate. We demonstrate that the signal intensities of numerous glycerophospho- and (glyco-)sphingolipids, as well as further compounds, are boosted by up to three orders of magnitude.

Results and Discussion

The layout of our PI source is sketched in Figure 1, and, in more technical detail, presented in Figure S1 of the electronic Supporting Information. In brief, the matrix-

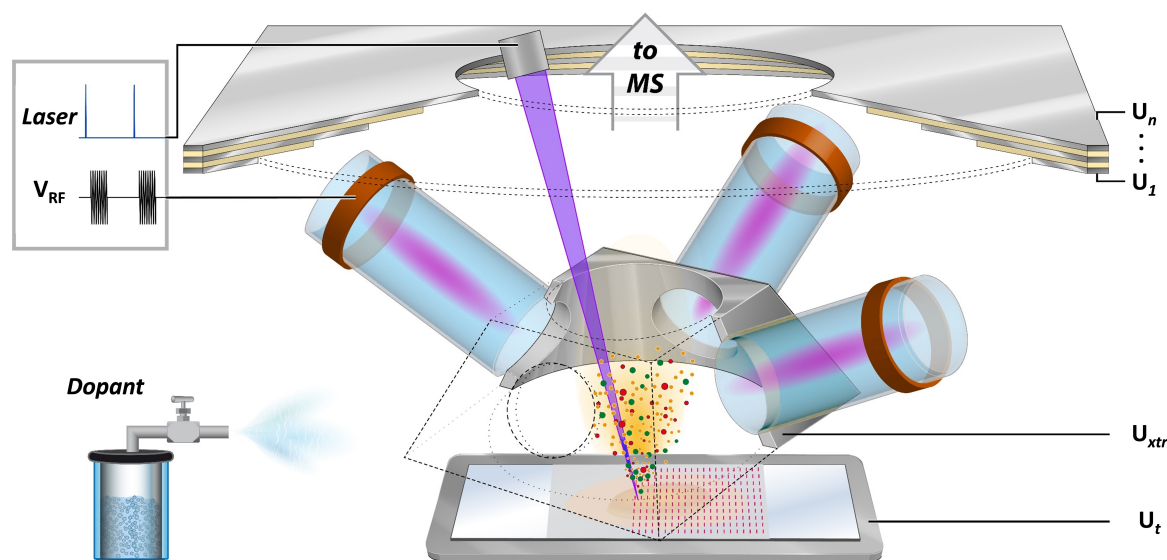


Figure 1. Schematic representation of the MALDI-SPICI ion source. Three symmetrically mounted Kr-discharge lamps are directed at an angle of 40° towards the particle plume generated by the pulsed MALDI laser from a matrix-coated sample. A symmetric ring electrode, supplied with an extraction voltage U_{xtr} , enables undisturbed ion extraction between the MALDI target at U , and the funnel electrodes at $U_{1,2,\dots,n}$. A custom-made class E amplifier drives the RF lamps at 13.560 MHz with V_{RF} and enables pulsed operation for optimal synchronization with the MALDI laser.

coated sample is irradiated by a series of ns-long UV laser pulses of 349 nm wavelength on a pixel-by-pixel basis, analogous to a classical MALDI-MSI experiment. To induce secondary ionization in the evolving MALDI plume, the ejected material is irradiated by three RF-Krypton discharge lamps operated at 13.560 MHz. The lamps are driven by custom-made electronics operated in pulsed mode with adjustable pulse width from a minimum of 70 μs (corresponding to the ignition time; see Figure 2b) to continuous operation.^[27] In the pulsed mode, the emission bursts of VUV radiation are synchronized with the MALDI laser by use of a delay generator (see below). The ion source is operated at fine-vacuum conditions of about 10 mbar of N_2 and dopant vapor (e.g., acetone) is introduced via a capillary system. Under these conditions, the mean free path of the gas compounds is in the order of a few micrometers, and radical primary ions, as generated by the SPI process, are subject to ample collisions with other neutral and charged constituents of the plume and background atmosphere such as matrix, analytes, dopant gas, and residual water vapor. Together, this enables numerous charge transfer reactions. Further instrumental detail as also data acquisition and

evaluation protocols are provided in the Experimental Section of the Supporting Information.

Optimizing Experimental Parameters

To characterize and optimize the performance characteristics of our PI module, we utilized thin sections of matrix-coated pig brain homogenate prepared as described earlier.^[14] 2,5-Dihydroxyacetophenone (DHAP) was used as the MALDI matrix in all reported experiments, which was shown to produce little background signals in MALDI-2 experiments.^[19] A few other common MALDI matrices like 2,5-dihydroxybenzoic acid (DHB) and norharmane were also tested. Compared with DHAP, the latter generally resulted in lower PI yields and higher background signal intensities. The laser pulse energy for the initial MALDI event was carefully adjusted for optimal MALDI performance with regard to ion yields of intact lipid species for MALDI and MALDI-SPICI, respectively. Similar to observations made for MALDI-2,^[14] SPICI requires considerably increased laser pulse energies for optimal ion yields as compared to classical MALDI. Even though the VUV-

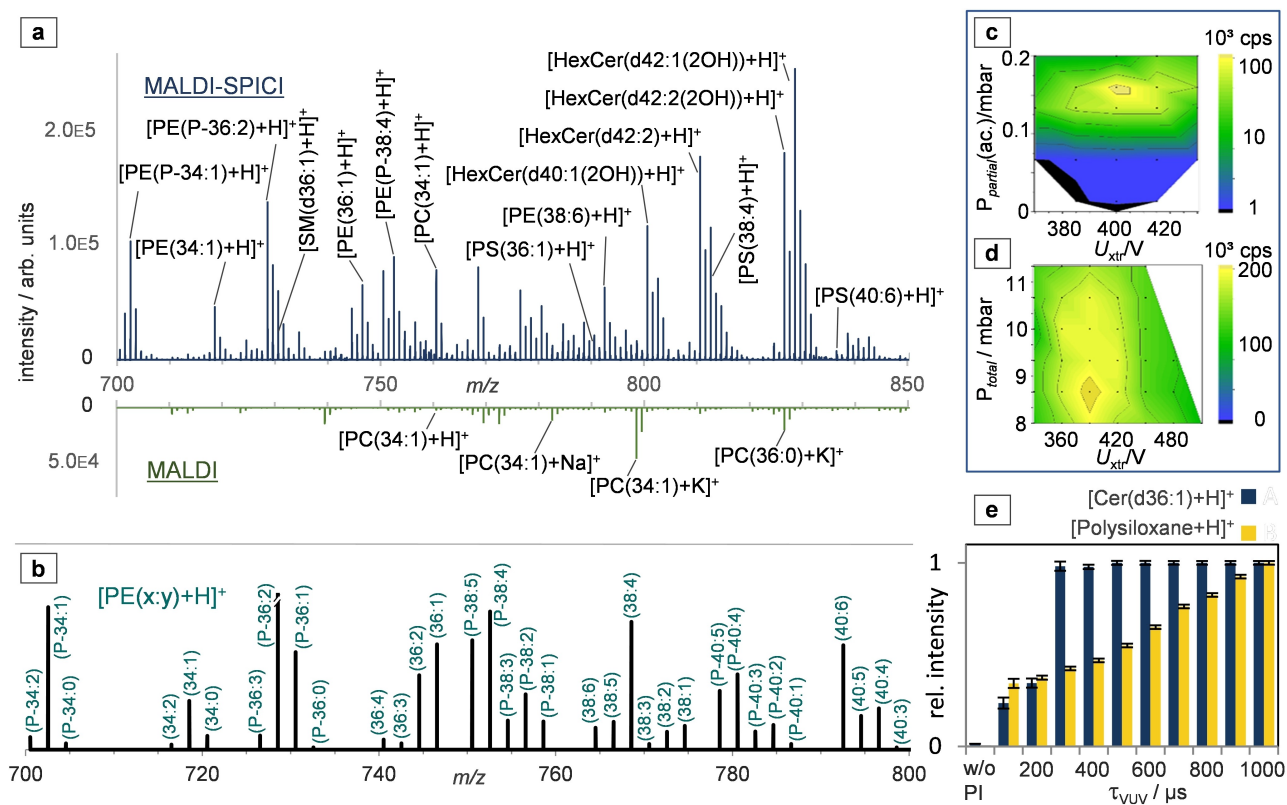


Figure 2. Parameter optimization. a) MALDI-SPICI (top) and MALDI-only (bottom) mass spectra of the central “phospholipid mass region” between 700 and 850 Da. The mass spectra were recorded from a DHAP-coated section of pig brain homogenate; 300 pixels were summed in each case according to a total of 90 000 laser shots. b) Extracted $[M+H]^+$ ion profiles for PE and PE plasmalogen species (averaged over 900 scans from three technical replicate measurements) assigned based on accurate mass; note that for the isobaric plasmalogens, only the plasmeryl (P-) variants are exemplarily annotated. c), d) Heat map showing the effect on the signal intensities of tentative $[\text{Cer}(\text{d}36:1)+\text{H}]^+$ of (c) the partial pressure of dopant (acetone) and U_{xtr} and (d) the total pressure and U_{xtr} ; black dots denote the experimental data points. e) Influence of the width of the VUV ignition pulse on the signal intensities of tentative $[\text{Cer}(\text{d}36:1)+\text{H}]^+$ and on polysiloxane-derived background ion signals ($[(\text{C}_2\text{H}_6\text{SiO})_n+\text{H}]^+$).

lamps as well as the employed laser system allow for the use of pulse repetition rates up to 5 kHz, the acquisition speed of the Q Exactive Plus Orbitrap mass analyzer limits the amenable scanning rates. An optimum of the overall signal intensities was identified at a frequency of 300 Hz for laser and synchronized VUV bursts and used as a constant setting for all experiments reported in the following.

Two mass spectra recorded from sections of pig brain homogenate with and without SPICI post-ionization are displayed in Figure 2a. The regular MALDI-MS measurement generated a total ion count (TIC) of $\approx 10^4$ counts per second (cps) for the m/z range from 450 to 1600 and upon averaging over 300 pixels. In the central “phospholipid region” between about m/z 700 to 850, we mainly registered Na^+ - and K^+ -adducts of major PCs, in accordance with general experience for this tissue type.^[14]

The MALDI-SPICI mass spectrum recorded over the same number of pixels reflects a substantially enhanced chemical coverage and a TIC that is increased by about two orders of magnitude. Next to different lipofoms of sphingolipids such as monohexosylceramides (HexCer), ceramides (Cer), and phosphatidylethanolamine ceramides (PE-Cer), numerous species of glycerophospholipids (GPL) other than PC (e.g., different lipofoms of phosphatidylethanolamines (PE), phosphatidylserines (PS), and plasmalogens) were detected with sizable signal intensities. All assignments are based on accurate mass, LIPID MAPS® data bank entries,^[29] and comparison with literature data^[20,30–33] (cf. Table S1 for m/z values and reference data; the data analysis^[34–37] is described in the Experimental Section, Supporting Information).

In general, MALDI-SPICI mass spectra largely resemble spectra recorded with laser-based MALDI-2. A qualitative comparison of mass spectra acquired with both PI techniques on the same instrument and a corresponding volcano plot are shown in Figure S2. Due to technical reasons, laser optics for material ejection as well ion optics for extraction differ between laser post-ionization and the prototype VUV ion source, currently hampering a more quantitative comparison between the two PI modalities. As with MALDI-2,^[14,15] intact protonated $[M+H]^+$ species were the main beneficiaries of the SPI-induced PI processes in the positive ion mode—the signals of sodium and potassium adducts, which form the base peaks for many classes of lipids in conventional MALDI-MSI spectra, were not amplified.^[14,38]

Overall, a total of about 200 different lipid species was tentatively assigned based on accurate mass in the m/z range from 450 to 1600 from pig brain homogenate samples (Table S1). As an example, the averaged signal intensities for all tentatively assigned protonated PE species (including PE plasmalogens) are plotted in Figure 2b.

As described in the following paragraphs, the effectiveness of SPICI post-ionization depends on a few basic experimental premises regarding the VUV-irradiation and the introduction of a dopant. These need to be adjusted for optimal results, including partial reduction of unwanted background signals enhanced by the SPICI process.

Optimizing Dopant Parameters

High yields for SPICI crucially depend on the use of a suitable dopant at carefully controlled conditions. In this study, we primarily used acetone. Measurements with toluene, anisole, and chlorobenzene as dopants resulted in the detection of similar $[M+H]^+$ species of the lipid analytes but generally generated lower signal intensities and higher chemical background. A comparison of mass spectra acquired with the four dopants is depicted in Figure S3. Peculiarly, no further classes of analytes, e.g., more hydrophobic compounds could be detected with increased intensity. We attribute this finding to a limited efficiency of laser desorption of these compounds due to the hydrophilic matrix.

Figure 2c illustrates the effect of the partial acetone dopant pressure on the ion signal registered at m/z 538.52, which we tentatively assigned as ceramide $[\text{Cer}(d36:1)+H]^+$ and exemplary chose as one of the numerous analyte ion signals benefitting from SPICI. The $[\text{Cer}(d36:1)+H]^+$ signal intensities drastically rise with increasing partial pressure of the dopant and reach a plateau at a value of about 0.16 mbar (we estimated the partial pressure as described in the Experimental Section). In a range from 8–12 mbar, the absolute pressure inside the ion source had only a minor influence on the general quality of the mass spectra (Figure 2d). Similarly, a variation of the extraction voltage U_{xt} did not have a major effect on the ion signal intensity over a range from 330–510 V (Figure 2d). However, to reproduce a high data quality with minimized signal fluctuation, it was crucial to realize stable conditions for the gas phase (buffer gas and partial dopant pressure) and the electric field.

Optimizing VUV-Irradiation

A pulsed operation of the Kr lamps that is carefully synchronized with the MALDI-process considerably improves the stability of ion signals and the quality of the acquired mass spectra: Next to signals of neutral molecules that are ablated in the MALDI event, signal intensities of chemical noise are sizably enhanced by SPICI with continuous VUV radiation—several polysiloxane- and plasticizer-derived signals are found prominently in the SPICI spectra (Figure S4). Most probably, this chemical noise originates primarily from the laboratory air that is introduced into the ion source, e.g., during sample loading. By shortening the duration of the VUV light burst, signal intensities of chemical noise are substantially reduced (Figure 2e). We found that the lamps can be ignited already with an electronic excitation pulse τ_{VUV} of 70 μs , which can be adjusted with our custom-made class E amplifier (see Supporting Information). Lipid ion counts were found to increase rapidly already with short bursts of VUV radiation, in contrast to signals of the chemical background. A plateau with an optimized signal-to-noise ratio (s/n-ratio) for lipid signals is reached at a pulse width between $\tau_{\text{VUV}} = 300\text{--}400 \mu\text{s}$ (Figure 2e). To ensure a steady measurement inside the plateau region, all experiments described in the following

were conducted with $\tau_{\text{VUV}} = 350 \mu\text{s}$. Next, we varied the delay between the MALDI laser pulse and the start of the VUV burst. Somewhat surprising, the delay did not show to be very relevant with regard to the efficiency of the SPICI process. These results stand in contrast to laser-based MALDI-2, in which neutrally ablated matrix molecules are directly photoionized about $10 \mu\text{s}$ after the MALDI event, and point to significant differences in the ionization processes.^[14,15]

Based on these findings, it could be reasoned that the dopant ions produced via SPI are relatively stable over the time between two laser bursts. After the initial material ejection, the MALDI-plume diffuses into the background gas, and charges are transferred from dopant ions to neutral analyte molecules. The pulse duration of the employed VUV bursts can be used to control the concentration of charged dopant inside the ion source and data suggest that optimal concentrations are reached for a pulse duration of around $350 \mu\text{s}$ (Figure 2e). At the same time, signals of chemical noise are continuously produced in the gas phase during VUV irradiation, which can decisively be mitigated by utilizing short VUV pulses.

Although reduced by the use of the pulsed irradiation and optimized partial pressure of the dopant, ions from chemical noise remained the dominating signals in the lower mass range in the positive ion mode (+)-SPICI mass spectra. To avoid saturation of the orbitrap, we recorded all presented (+)-MALDI-SPICI-MSI measurements with a lower cut-off at m/z 450. The following analytical MALDI-SPICI-MSI experiments were furthermore recorded with the optimized conditions of $P_{\text{total}} = 8.5 \text{ mbar}$, $P_{\text{partial}}(\text{acetone}) = 0.16 \text{ mbar}$, $U_{\text{xt}} = 400 \text{ V}$, and $U_{\text{t}} = 400 \text{ V}$.

MALDI-SPICI-MSI

Making use of the optimized parameter settings, we next explored the potential of our method for MALDI-MS imaging of mouse brain sections. Selected ion images recorded from a coronal mouse brain section are plotted in Figure 3. The data visualize the major increase in the analytic depth upon the use of MALDI-SPICI and the shift of ion species towards protonated $[M+H]^+$ species. Note that for the lipid classes depicted in Figure 3, signals of protonated and sodiated/potassiated species were not detected or only with minor intensities with regular MALDI-MSI; similar to the findings for porcine brain homogenate (Figure 2a).

To evaluate the stability and long-term effects of the pulsed VUV light generation in the vacuum chamber, we chose to measure a large tissue section with a long transient time of the Orbitrap mass analyzer of 0.5 s at a mass resolving power of 140 000 (at m/z 200). The resulting data presented in Figure 3 were recorded over a total measurement time of 42 hours and are depicted without signal normalization. This demonstrates high robustness in the signal generation in MALDI-SPICI over such extended periods of time.

As compared with regular MALDI, SPICI post-ionization substantially extends the analytical capabilities, allowing for a more detailed characterization of the distribution of numerous lipid classes in different tissue regions like the white matter or the molecular layer in the case of mouse cerebellum. The benefit of the high mass resolving power that is provided by the Q Exactive Plus mass analyzer is demonstrated exemplarily in the zoom-in to a narrow mass window between m/z 774.4 and 774.8 (Figure 3p). Within a mass window of $<0.2 \text{ Da}$ alone, we registered six different ion species with acceptable separation. The (partly) differential distribution of the six compounds in the brain is shown in panels g-m of Figure 3. Overall, based on accurate mass and comparison with databases and the pertinent literature, we could tentatively assign about 250 different lipid species using MALDI-SPICI-MSI (Table S1).

As a second example, selected ion images recorded from a mouse kidney section are displayed in Figure S5. Exemplarily, we tentatively assigned high intensity signals to protonated species of Cer(d42:1), PS(38:4) and Cardiolipin (CL)(76:6), in the cortex, Hex₂Cer(d32:1) in the medulla, and lyso-(L-)PE(18:1) in the Calyx/Pelvis.

The high signal intensities that are obtained for many analyte species with MALDI-SPICI enable an efficient tandem MS analyses for structure elucidation. To demonstrate this important feature and further characterize the increased depth of molecular coverage, we made use of data-dependent acquisition MS/MS (DDA-MS/MS).^[33] In the conducted "Top4 experiment", one full scan pixel is followed on the sequential four pixels by four automated MS/MS experiments of the highest signals with a dynamic exclusion time of 9 s per distinct m/z value. Figure 4 shows a mouse brain section measured with Top4-DDA that was adjacent to the tissue section used to produce the MS¹ data of Figure 3. Figure 4a depicts average MS/MS spectra acquired for three exemplary m/z values. The MS images of the respective signal intensity distributions in the full scan mass spectra are shown in Figure 4b. In total, we obtained lipid species confirmation and additional molecular species levels for 40 tentatively assigned lipid species with the DDA experiments (Table S1). Importantly, these include species from many GPL other than PC and ceramide species that commonly are not detected with sufficient intensity for tandem MS in (+)-MALDI-MSI. A more comprehensive lipid characterization, however, would require cross-confirmation experiments such as, e.g., laser-micro dissection in combination with liquid chromatography (LC)-MS/MS analysis^[39] or ion mobility separation.^[22]

Negative-Ion Mode

A set of mass spectra and ion images was also recorded from DHAP-coated tissue sections in the negative ion mode. Testing MALDI matrices in the negative ion mode, the use of 2,5-DHAP yielded higher lipid ion counts and lower matrix signal intensities compared to norharmane. Notably, we obtained optimal MS results with similar settings for the operation of the pulsed RF lamp and acetone

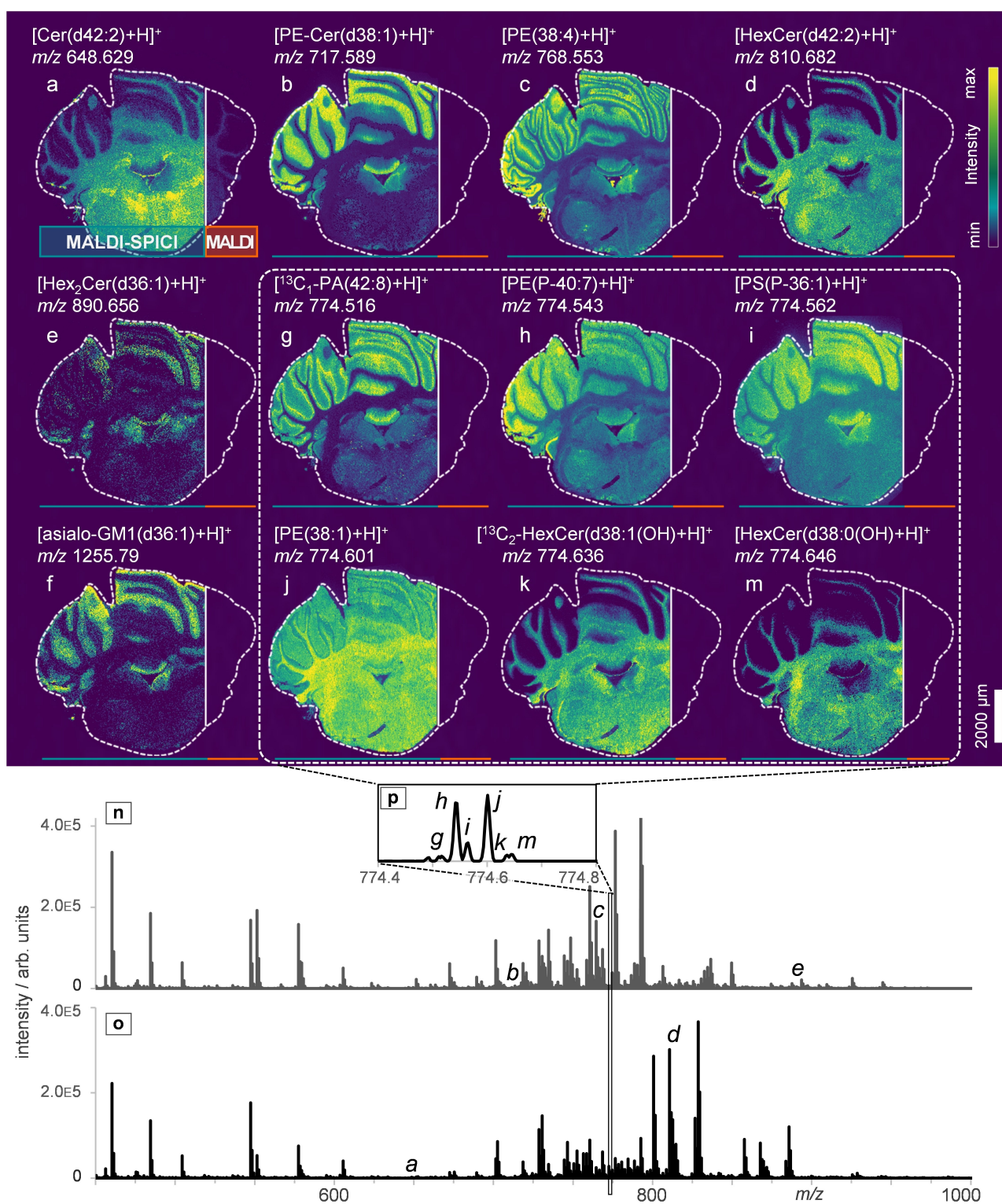


Figure 3. MALDI-SPICI-MS imaging of a coronal mouse brain section recorded in the positive ion mode. Upon MALDI-SPICI (left side of the images (a)–(m)), distinct distributions within the white and gray matter of the cerebellum and the medulla are obtained for numerous analytes, most of which are not detected with regular MALDI-MSI (right side). Data were recorded over 42 h at a pixel size of 16 μm , a mass resolving power Res_m of 140000 and with $f_{\text{rep}} = 300$ Hz. Tentative assignments as denoted in the figure are based on accurate mass and literature data. n, o): exemplary single-pixel MALDI-SPICI mass spectra recorded from (n) the molecular layer and (o) the white matter. p) Zoom-in spectrum showing signals of 1000 averaged pixels in a 0.4 Da-wide window. GM1 = monosialotetrahexosylganglioside, PA = phosphatidic acid.

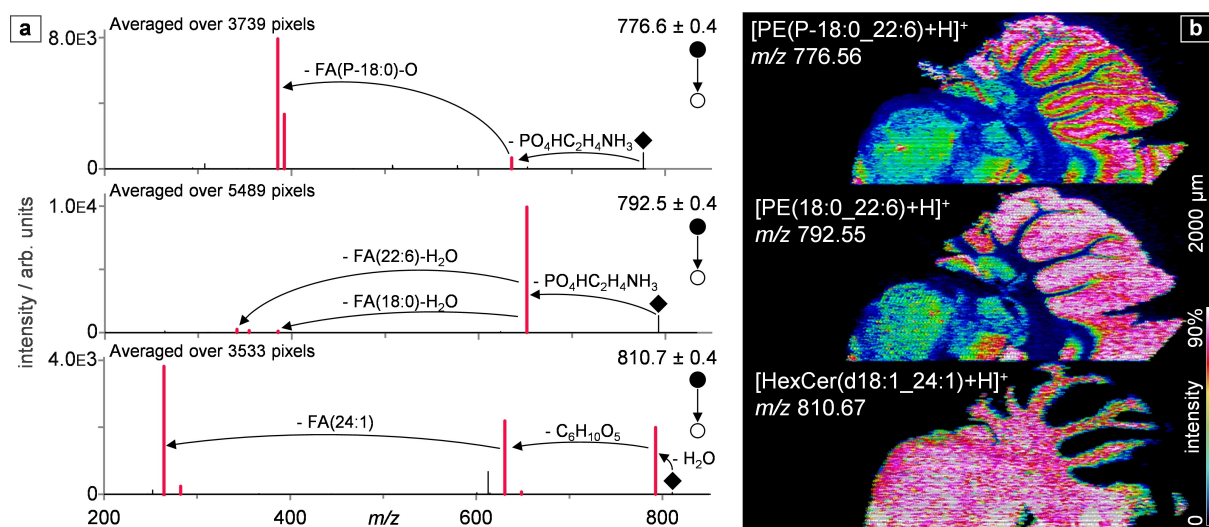


Figure 4. MALDI-SPICI-DDA-(MS/MS)-MSI of a coronal mouse brain section. a) Exemplary MS/MS spectra averaged over the number of pixels indicated in the spectra; red signals represent fragments that confirm the lipid's molecular species, \blacklozenge mark the $[M+H]^+$ precursor ions. b) MSI signal intensity distribution of the identified lipids in the sequential full scans (extrapolated to a five-pixel wide block; see Experimental Section, Supporting Information). Data were recorded as a Top4-DDA experiment at a pixel size of $16\ \mu\text{m}$ and $f_{\text{rep}} = 300\ \text{Hz}$. The mass resolution for the full scan was $\text{Res}_m(\text{MS}^1)$: 140 000 (defined for m/z 200) and for the tandem-MS it was $\text{Res}_m(\text{MS}^2)$: 70 000. MSI data are shown without normalization.

dopant supply as in the positive ion mode; specifically, optimized settings as determined with pig brain homogenate sections were: $P_{\text{total}} = 8.5\ \text{mbar}$, $P_{\text{partial}}(\text{acetone}) = 0.2\ \text{mbar}$, $U_{\text{xt}} = -360\ \text{V}$, $U_{\text{target}} = -400\ \text{V}$, $\tau_{\text{VUV}} = 350\ \mu\text{s}$. We hence used these parameters for all shown negative ion mode (–)MALDI-SPICI-MSI experiments. As in the positive ion mode, the data widely resemble those acquired with laser-based MALDI-2^[14,20,38] with regard to both the boosted chemical coverage/signal intensities (e.g., of numerous glycerophospho- and sphingolipids) as well as to the type of predominantly recorded ions (i.e., $[M-H]^-$; Figure S6). Measuring brain homogenate within a Top4-DDA-MS/MS MALDI-SPICI experiment, a total of 56 lipid species annotations could be confirmed by unambiguous fragmentation (c.f. Table S1).

Notably, in contrast to the positive ion mode, chemical noise signals are detected with lower intensity in the negative ion mode and were suppressed to an almost negligible intensity when pulsed lamp operation and partial pressure of the dopant $P_{\text{partial}}(\text{acetone}) > 0.1\ \text{mbar}$ were applied (data not shown). Semi-volatile free fatty acids were, however, recorded with high intensity in the mass range of $m/z < 320$ (see Figure S7). Consequently, negative ion mode MALDI-SPICI-MS can more readily be used to cover smaller metabolites. The less effective ionization of compounds in the surrounding gas phase—background signals—is in accordance with the selected ionization efficiencies reported in the literature for APPI-MS in the negative mode.^[25] In MALDI-PI, however, the high coverage of the lipid profile in the negative ion mode stands in contrast to the selective ionization pathways described for negative ion mode APPI-MS. This can be viewed as an indication for different ionization mechanisms of SPICI in the dense micro-reaction volume of the expanding MALDI

plume compared to those reported for APPI. Another indicator for this assumption is the observation that SPICI with toluene or anisole as a dopant did not yield molecular ions but (de-)protonated ion species (see Figure S3), whereas these dopants are known for electron-transfer reactions in APPI.^[25] Further experiments will be needed to explore the ionization mechanisms for these charge-transfer dopants.

Selected ion images from a (–)MALDI-SPICI-MSI experiment of a coronal mouse brain section are shown in Figure S8. Numerous signals can tentatively be assigned to deprotonated species of cerebral lipids. The broad spectrum of detected lipid species, for example, ranging from cyclic lyso-GPL such as $[\text{cLPA}(16:0)-H]^-$ (m/z 391.23; Figure S8a) to high masses of monosialotetra-hexosylganglioside $[\text{GM1}(d36:1)-H]^-$ (m/z 1544.87; Figure S8e). Similar to the positive ion mode, the majority of lipid ion signals was obtained only upon PI. In total, based on accurate mass, we registered about 270 different lipid species from the brain tissue in the m/z range from 320 to 1600 in the negative ion mode.

Ionization Mechanism

Based on the fundamental and analytical results, we reason that the VUV-induced post-ionization takes place only at the interplay of the laser plume, VUV pulse, and dopant altogether.

Without laser irradiation, no desorption was monitored and no carry-over between pixels is observable in the MS images (Figure 3). No morphological degradation was visible on the tissue samples or the matrix layer apart from laser ablation marks after imaging experiments. To investigate a possible chemical degradation caused by the undirected

VUV irradiation of the tissue, we compared the first and the last mass spectra acquired from brain homogenate with MALDI-SPICI as also mass spectra generated with regular MALDI before and after 30 min of tissue irradiation. Fold change plots generated from the data of these measurement points did not show major variations in signal intensities (Figure S9). Accordingly, a close inspection of mass spectra generated early and late during the imaging run did not reveal any chemical degradation to well-known products such as, e.g., cleaved fatty acid chains, formal PA species (loss of a head group of a PC/PE species), or oxidation products. We speculate that the impermeable matrix layer shields the tissue against VUV light as well as reactive molecules from the gas phase. Yet, degradation effects cannot be fully excluded and should be considered for unknown complex sample systems.

To gain further insights into the ionization mechanisms as well as into possible fragmentation pathways, we conducted a series of experiments in the (+) ion mode with two phospholipid standards, namely PS(16:0/18:1) and PC(16:0/18:1), and by use of deuterated DHAP matrix, acetone- d_6 , and D_2O , respectively. Lipid standard solutions were evenly sprayed onto histological glass slides and subsequently coated with matrix by sublimation. MALDI-SPICI spectra were generated by averaging over 60 pixels (1 min) per parameter set. Further experimental details are described in the Experimental Section, Supporting Information.

The use of perdeuterated acetone as a dopant resulted in no visible changes in the mass spectra as compared to regular acetone. In particular, we observed no auto-deuteration of the dopant and thus no deuteration of the

analytes; acetone was recorded solely as protonated species (Figure S10). These findings are in line with results from APPI experiments with perdeuterated acetone dopant.^[40]

Using deuterated DHAP matrix and regular acetone as the dopant, the recorded MALDI-only mass spectra revealed differences to those obtained with the regular matrix. Expectedly, an isotope distribution with different degrees of hydrogen-deuterium-exchange (HDX) was monitored with the signal for $[PS(34:1)-d_2+D]^+$ forming the base peak in the mass spectrum (Figure 5a1). As the VUV lamps were switched on, the picture changed entirely (Figure 5a2). No HDX products were visible in the MALDI-SPICI mass spectra and the $[M+H]^+$ signal of PS(34:1) formed the base peak along with the regular isotope pattern.

We tentatively attribute this finding to a high degree of chemical interaction in the confined plume between photo-activated acetone, matrix, and analyte ions and molecules. This appears to lead to complete deuterium-hydrogen-exchange (DHX) towards the large reservoir of acetone within the overall SPICI process.

Using D_2O , which we introduced into the ion source with $P_{\text{partial}} \leq 0.04$ mbar in addition to the regular acetone dopant (see Experimental Section, Supporting Information), moderate levels of HDX in the gas phase resulted in the detection of deuterated PS in the case of conventional MALDI. The signal for $[PS(34:1)-d_1+D]^+$ formed the base peak of an isotopic distribution pattern in the mass spectrum (Figure 5b1). This result is generally in line with MALDI-MS data published by Kostyukevich et al. of a dual ion funnel device similar to the one used in our study. These authors reported HDX of up to four labile hydrogen atoms

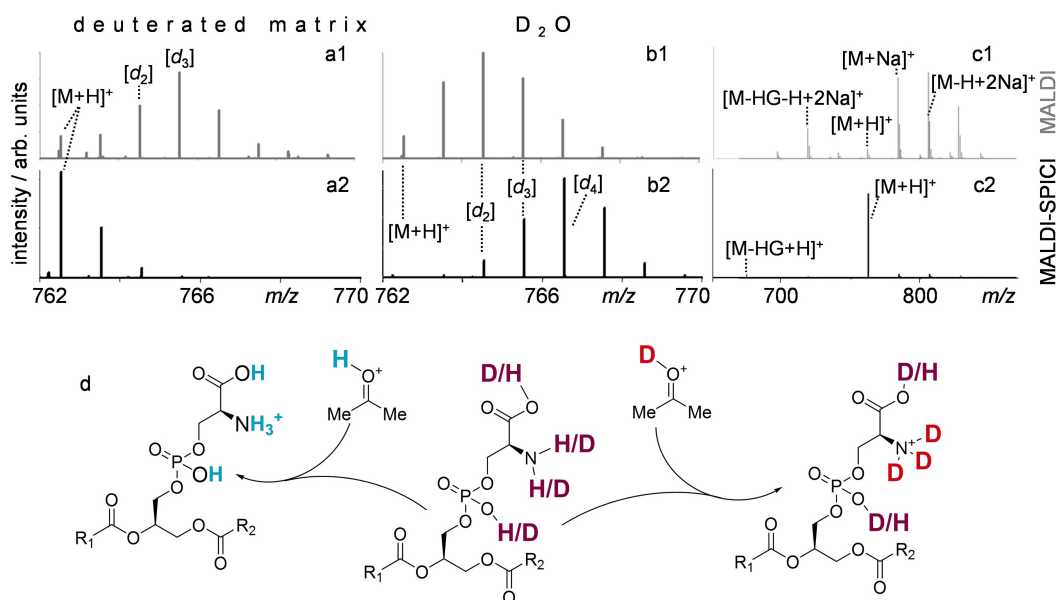


Figure 5. Deuteration and fragmentation experiments with PS(16:0/18:1) standard to reveal details of the (+)-SPICI ionization pathways. Upper spectra are measured with regular MALDI, lower spectra with MALDI-PI; Res_m : 280000. a1), a2) Zoom-in of mass spectra using the deuterated DHAP matrix. b1), b2) Zoom-in of mass spectra using a D_2O -enriched atmosphere. c1), c2) Mass spectra without deuterated components. d) Reaction scheme showing the suggested main gas-phase ionization step with protonated and deuterated acetone, respectively. HG = head group ($C_3H_5O_2N$), $R_1=C(16:0)$, $R_2=C(18:1)$ hydrocarbon chains.

of PS after the introduction of D₂O vapor in the fine vacuum atmosphere.^[41]

In our study, upon the use of SPICI post-ionization, the highest degree of HDX was observed, with [PS(34:1)-d₃+D]⁺ now forming the base peak (Figure 5b2).

Ionization Pathway

Together, these findings suggest that the critical proton (or deuteron) donor in the MALDI-SPICI ionization event in the positive ion mode is not the MALDI matrix. Rather, ubiquitous protic molecules like residual H₂O in the gas phase appear to be pivotal contributors. High concentrations of (acetone) dopant molecules appear to mediate the proton transfer after initial excitation by the VUV pulse. For acetone, this happens presumably by the formation of an intermediate state of a formally protonated carboxylic group. The suggested main gas-phase ionization step with protonated and deuterated acetone, respectively, is shown in Figure 5d. It should be emphasized that the hydrogen atoms of the acetone methyl groups do not directly take part in the proton transfer reaction.

The results from analogous deuteration experiments with the PC(34:1) standard are summarized in Figure S11. PCs contain only one labile hydrogen atom, thus, we observed only single deuteration, formally forming an [M+D]⁺ ion. With regard to all other features, the results obtained with the PC standard fully resemble those obtained with PS standard described above: Regular MALDI-MS performed with deuterated matrix yielded [PC(34:1)+D]⁺, while the utilization of PI led to DHX and the formation of [M+H]⁺. In a D₂O-enriched gas atmosphere, the PI step led to the formation of intensive [PC(34:1)+D]⁺ signals.

Furthermore, the standard spectra did not reveal any degradation of the lipid standards neither by the VUV irradiation nor in the chemical interplay with the dopant.

Degree of Fragmentation

The degree of fragmentation reactions in conventional MALDI and MALDI-SPICI may to first-order be assessed by the loss of the headgroup (HG; C₃H₅O₂N) from the PS standard (Figure 5c1). The dominant fragmentation product [M-HG-H+2Na]⁺ is detected with a relative intensity of ≈40% compared to the intact precursor—note that the relatively high degree of fragmentation,^[9] in this case, is due to the high laser fluence, which was set to the same value as used for the MALDI-SPICI experiments. Upon PI, solely the protonated ion species of the PS increase in intensity; the [M+H]⁺ signal is amplified by about two orders of magnitude. The corresponding [M-HG+H]⁺ fragment is detected with only 10% relative intensity compared to the intact [M+H]⁺ species (Figure 5c2). The data suggest that the detected fragment signals are mostly the result of the post-ionization of fragments generated in the initial MALDI event. Similar findings of low fragmentation rates were reported for laser-based MALDI-2.^[14]

The results from the analogous experiments with the PC(16:0/18:1) standard are shown in Figure S11. Also here, the PI process specifically enhanced the generation of protonated species, and only a minute degree of fragmentation of about 20% relative to the intact [M+H]⁺ species is observed.

Conclusion

We present the implementation of pulsed RF-Kr discharge lamps in an ion funnel ion source for “soft and simple” PI of glycerophospho- and (glyco)sphingolipids and numerous further compounds in high-resolving MALDI-MS imaging. Upon use of acetone dopant, MALDI-SPICI yields ion boosts of up to three orders of magnitude of [M+H]⁺ resp. [M-H]⁻ species. The generated mass spectra are generally similar to those obtained with laser-based MALDI-2 and reflect a very low if not fully absent degree of analyte fragmentation during the PI step.

Using deuterated components, we present a glimpse into the secondary ionization mechanisms of SPICI. These data suggest a rather complex chemical interplay in the dense micro reaction environment different from the mechanism of MALDI-2. The method should therefore neither be described as matrix-assisted nor as a direct SPI process.

Whereas the analyte signal boosts are readily achieved over the full mass range in the negative ion mode, an optimized ion source design may in the future help to reduce the currently high chemical background observed in the positive ion mode. Future experiments will elucidate the PI efficiency of MALDI-SPICI for the detection of endogenous compounds other than lipids and exogenous substances such as, e.g., pharmaceuticals. As the MALDI matrix is not actively involved in the ionization mechanism, matrix-free LDI techniques, as well as the use of different dopants, could further broaden the range of analyte classes amenable to the method.

Our in-house developed SPICI module enables operation with pulse repetition rates of several kHz and could readily be combined with laser systems and mass spectrometers exceeding laser repetition rates of 1 kHz^[22]. Coupling with laser repetition rates in the MHz range is possible when lamps are operated in the continuous mode.

All features together could render the presented MALDI-SPICI methodology a useful addition to the bioanalytical toolbox for mass spectrometry imaging and a valuable and low-cost alternative to MALDI-2.

Acknowledgements

We thank Ansgar Korf (Bruker Daltonik) for assistance with MZmine 2 software, Sara Tortorella (Molecular Horizon) for providing LipostarMSI software, Willi Kramer (University Hospital Münster) for production of Figures 1, S1, and the Table of Contents graphic, Marcel Niehaus for assistance with designing the ion source, Fabian Eiersbrock for help with developing an optimal sample preparation

protocol, Jan Schwenzfeier for support with the data analysis software, and Alexander Potthoff, Gottfried Pohlentz, and Michael Mormann for numerous helpful discussions. Financial support by the German Research Foundation (DFG; grants DR416/12-1 and SO476/3-1, project number 290343045, and DR416/13-1 and SO476/4-1, project number 326945247; both to K.D. and J.S.) is gratefully acknowledged. We mourn the early passing of our co-author, colleague, and friend Ulrich Röhling, who decisively contributed to the success of the presented work. Open Access funding enabled and organized by Projekt DEAL.

Conflict of Interest

The authors declare no conflict of interest.

Data Availability Statement

The data that support the findings of this study are available from the corresponding author upon reasonable request.

Keywords: Analytical Methods · Lipidomics · MALDI-MS Imaging · Mass Spectrometry · Post-Ionization

-
- [1] A. R. Buchberger, K. DeLaney, J. Johnson, L. Li, *Anal. Chem.* **2018**, *90*, 240.
- [2] T. Züllig, H. C. Köfeler, *Mass Spectrom. Rev.* **2021**, *40*, 162–176.
- [3] K. Ščupáková, B. Balluff, C. Tressler, T. Adelaja, R. M. A. Heeren, K. Glunde, G. Ertaylan, *Clin. Chem. Lab. Med.* **2020**, *58*, 914.
- [4] J. G. Swales, G. Hamm, M. R. Clench, R. J. Goodwin, *Int. J. Mass Spectrom.* **2019**, *437*, 99.
- [5] A. Palmer, D. Trede, T. Alexandrov, *Metabolomics* **2016**, *12*, 422.
- [6] M. Kompauer, S. Heiles, B. Spengler, *Nat. Methods* **2017**, *14*, 90.
- [7] M. Niehaus, J. Soltwisch, M. E. Belov, K. Dreisewerd, *Nat. Methods* **2019**, *16*, 925.
- [8] K. N. Robinson, R. T. Steven, A. M. Race, J. Bunch, *J. Am. Soc. Mass Spectrom.* **2019**, *30*, 1284.
- [9] J. Schiller, R. Süß, J. Arnhold, B. Fuchs, J. Leßig, M. Müller, M. Petković, H. Spalteholz, O. Zschörnig, K. Arnold, *Progress Lipid Res.* **2004**, *43*, 449.
- [10] M. S. Boskamp, J. Soltwisch, *Anal. Chem.* **2020**, *92*, 5222.
- [11] L. Hanley, R. Wickramasinghe, Y. P. Yung, *Annu. Rev. Anal. Chem.* **2019**, *12*, 225.
- [12] X. Ding, K. Liu, Z. Shi, *Mass Spectrom. Rev.* **2021**, *40*, 566–605.
- [13] E. A. Elia, M. Niehaus, R. T. Steven, J.-C. Wolf, J. Bunch, *Anal. Chem.* **2020**, *92*, 15285.
- [14] J. Soltwisch, H. Kettling, S. Vens-Cappell, M. Wiegelmann, J. Müthing, K. Dreisewerd, *Science* **2015**, *348*, 211.
- [15] A. Potthoff, K. Dreisewerd, J. Soltwisch, *J. Am. Soc. Mass Spectrom.* **2020**, *31*, 1844.
- [16] A. Potthoff, O. Minte, K. Dreisewerd, J. Soltwisch, *J. Am. Soc. Mass Spectrom.* **2022**, *33*, 315.
- [17] F. P. Y. Barré, M. R. L. Paine, B. Flinders, A. J. Trevitt, P. D. Kelly, R. Ait-Belkacem, J. P. Garcia, L. B. Creemers, J. Stauber, R. J. Vreeken et al., *Anal. Chem.* **2019**, *91*, 10840.
- [18] A. Bednařík, S. Bölsker, J. Soltwisch, K. Dreisewerd, *Angew. Chem. Int. Ed.* **2018**, *57*, 12092; *Angew. Chem.* **2018**, *130*, 12268.
- [19] E. U. Brockmann, D. Steil, A. Bauwens, J. Soltwisch, K. Dreisewerd, *Anal. Chem.* **2019**, *91*, 15081.
- [20] A. P. Bowman, J. F. J. Bogie, J. J. A. Hendriks, M. Haidar, M. Belov, R. M. A. Heeren, S. R. Ellis, *Anal. Bioanal. Chem.* **2020**, *412*, 2277.
- [21] B. Heijs, A. Potthoff, J. Soltwisch, K. Dreisewerd, *Anal. Chem.* **2020**, *92*, 13904.
- [22] J. Soltwisch, B. Heijs, A. Koch, S. Vens-Cappell, J. Höhndorf, K. Dreisewerd, *Anal. Chem.* **2020**, *92*, 8697.
- [23] L. Hanley, R. Zimmermann, *Anal. Chem.* **2009**, *81*, 4174.
- [24] Y. J. Shi, R. H. Lipson, *Can. J. Chem.* **2005**, *83*, 1891.
- [25] T. J. Kauppila, J. A. Syage, T. Benter, *Mass Spectrom. Rev.* **2017**, *36*, 423.
- [26] J. A. Syage, M. A. Hanning-Lee, K. A. Hanold, *Field Analyt. Chem. Technol.* **2000**, *4*, 204.
- [27] C. Bookmeyer, J. Soltwisch, U. Röhling, K. Dreisewerd, *ChemPlusChem* **2020**, *85*, 1559.
- [28] H. Hsu, C.-K. Ni, *Appl. Sci.* **2018**, *8*, 699.
- [29] E. Fahy, M. Sud, D. Cotter, S. Subramaniam, *Nucleic Acids Res.* **2007**, *35*, W606–W612.
- [30] E. Cífková, M. Holčápek, M. Lísa, *Lipids* **2013**, *48*, 915.
- [31] J. Choi, T. Yin, K. Shinozaki, J. W. Lampe, J. F. Stevens, L. B. Becker, J. Kim, *Mol. Cell. Biochem.* **2018**, *442*, 187.
- [32] T. Zhang, S. Chen, X. Liang, H. Zhang, *Anal. Bioanal. Chem.* **2015**, *407*, 6543.
- [33] S. R. Ellis, M. R. L. Paine, G. B. Eijkel, J. K. Pauling, P. Husen, M. W. Jervelund, M. Hermansson, C. S. Ejsing, R. M. A. Heeren, *Nat. Methods* **2018**, *15*, 515.
- [34] M. C. Chambers, B. Maclean, R. Burke, D. Amodei, D. L. Ruderman, S. Neumann, L. Gatto, B. Fischer, B. Pratt, J. Egerton et al., *Nat. Biotechnol.* **2012**, *30*, 918.
- [35] L. Goracci, S. Tortorella, P. Tiberi, R. M. Pellegrino, A. Di Veroli, A. Valeri, G. Cruciani, *Anal. Chem.* **2017**, *89*, 6257.
- [36] T. Pluskal, S. Castillo, A. Villar-Briones, M. Oresic, *BMC Bioinf.* **2010**, *11*, 395.
- [37] A. Korf, V. Jeck, R. Schmid, P. O. Helmer, H. Hayen, *Anal. Chem.* **2019**, *91*, 5098.
- [38] S. R. Ellis, J. Soltwisch, M. R. L. Paine, K. Dreisewerd, R. M. A. Heeren, *Chem. Commun.* **2017**, *53*, 7246.
- [39] F. B. Eiersbrock, J. M. Orthen, J. Soltwisch, *Anal. Bioanal. Chem.* **2020**, *412*, 6875.
- [40] C.-R. Raddatz, M. Allers, A. T. Kirk, S. Zimmermann, *Int. J. Ion Mobility Spectrom.* **2018**, *21*, 49.
- [41] Y. Kostyukevich, G. Vladimirov, E. Stekolschikova, D. Ivanov, A. Yablokov, A. Zhrebker, S. Sosnin, A. Orlov, M. Fedorov, P. Khaitovich et al., *Anal. Chem.* **2019**, *91*, 13465.

Manuscript received: February 9, 2022

Accepted manuscript online: June 21, 2022

Version of record online: July 14, 2022